

Covalent Organic Nanosheets for Bioimaging

**Gobinda Das,^{[a]‡} Farah Benyettou,^{[a]‡} Sudhir Shrama,^[b] Thirumurugan Prakasam,^[a]
Felipe Gándara,^[c] Victor A. de la Peña -O'Shea,^[d] Na'il Saleh,^[e] Renu Pasricha,^[a]
Ramesh Jagannathan,^[b] Mark A Olson^[f] and Ali Trabolssi^{*,[a]}**

^a Chemistry Program, New York University Abu Dhabi (NYUAD), Experimental Research Building (C1), Saadiyat Island, United Arab Emirates

^b Engineering Division, New York University Abu Dhabi (NYUAD), Experimental Research Building (C1), Saadiyat Island, United Arab Emirates

^c Materials Science Factory, Instituto de Ciencia de Materiales de Madrid – CSIC, Sor Juana Inés de la Cruz 3, 28049 Madrid, Spain

^d Photoactivated Processes Unit, IMDEA Energy, Avd. Juan de la Sagra 3, Mostoles 28935, Madrid, Spain

^e Chemistry Department, College of Science, United Arab Emirates University, P.O. Box 15551, Al-Ain, United Arab Emirates

^f School of Pharmaceutical Science and Technology, Tianjin University, China

‡ Equal Contribution

Supporting Information

- S1: General Material and Methods
- S2: Synthetic procedure
- S3: Fourier Transform Infrared (FTIR) Spectroscopy of the Synthesized TTA-DFP COF and TTA-DFP CONs Materials and their Precursors
- S4: Thermogravimetric Analyses of TTA-DFP COF and TTA-DFP CONs
- S5: Room Temperature PXRD Patterns of TTA-DFP CONs
- S6: Pore Size Distribution of TTA-DFP COF.
- S7: AFM Height Profiles of TTA-DFP COF and TTA-DFP CONs
- S8: Room Temperature PXRD Patterns of TTA-DFP CONs
- S9: Dynamic Light Scattering (DLS) Characterization
- S10: AFM Height Profiles of TTA-DFP COF and TTA-DFP CONs
- S11: HRTEM and AFM Analysis of TTA-DFP COF and TTA-DFP CONs
- S12: Luminescent Study of TTA-DFP COF, TTA-DFP CONs and TTA-Monomer.
- S13: Plane Wave Density Functional Theory (PW-DFT) Analysis
- S14: Band Gap Calculations for UV-vis Spectra
- S15: The Frontier Molecular orbital Distributions of TTA-DFP CONs Fragment by DFT Calculations
- S16: Biological Studies

S1. General Materials and Methods

All reagents and starting materials were purchased from Sigma-Aldrich and used without further purification. The precursor, 2,6-diformylpyridine (DFP) was synthesized according to the published procedure with no modifications. Deionized water was used from Millipore Gradient Milli-Q water purification system. Thin-layer chromatography (TLC) was performed on silica gel 60 F254 (E. Merck). The plates were inspected under the UV light. Column chromatography was performed on silica gel 60F (Merck 9385, 0.040–0.063 mm). Routine nuclear magnetic resonance (NMR) spectra were recorded at 25 °C on a Bruker Avance spectrometer, with a working frequency of 500 and 125 MHz for ^1H , and 151.0 MHz for ^{13}C nuclei. All chemical shifts are reported in ppm relative to the signals corresponding to the residual non-deuterated solvents (CD_3CN : $\delta = 1.94$ ppm, CD_3OD : $\delta = 3.31$ ppm, D_2O : $\delta = 4.97$ ppm and DMSO-d_6 : $\delta = 2.50$ ppm). Coupling constant values (J) are given in hertz (Hz), the multiplicity is abbreviated in the following way: s (singlet) and d (doublet). Fourier transform infrared (FTIR) studies were carried out on the Agilent 670-IR spectrometer. Thermogravimetric analysis (TGA) was performed on TA SDT Q600. Scanning electron microscopy (SEM) images were obtained from FEI Quanta 450FEG. The topography of the self-templated samples was analyzed by dynamic atomic force microscopy (5500 Atomic Force Microscope; Keysight Technologies Inc., Santa Rosa, CA). We acquired topography, phase and amplitude scans simultaneously. Silicon cantilevers (NanosensorsTM, Neuchatel, Switzerland) with resonant frequencies of 250–300 kHz and force constants of 100–130 Nm^{-1} were used. The set point value was kept at 2.5V. AFM scans were collected at 1024 points/lines with scan speed of 0.20 at fixed scan angle of 0°. Scan artifacts were minimized by acquiring a typical scan at an angle of 90° under identical image acquisition parameters. We used GwyddionTM free software (version 2.47), an SPM data visualization and analysis tool for post-processing the AFM scans. Size and morphology of the nanoparticles were determined with a TEM (FEI-Titan 300) microscope. Samples were prepared on a carbon-coated copper grid. A drop of dispersed polymeric network was spotted on the grid and allowed to dry overnight. UV-Vis studies were carried out on the Cary 5000 UV-Vis-NIR spectrophotometer. All UV-Vis spectra were recorded at room temperature in a quartz cell with 10 mm path length. N_2 adsorption/desorption isothermal curves were both recorded at 273 K up to 1 bar using a manometric Micromeritics 3Flex gas sorption analyzer along with a PolyScience Circulating bath (50:50 vol%, water:ethylene glycol mixture) for maintaining constant temperature during the experiments. Powder X-ray diffraction (PXRD) measurements were carried out using the PANalytical X'Pert PRO MP X-ray diffractometer consisting of a focusing elliptical mirror and a fast high resolution detector (PIXCEL) with the radiation wavelength of 0.15418 nm.

The solid-state steady-state and time-resolved fluorescence measurements of polymers solid state and as a suspension (about 1 milligrams in 10 ml solvent) in different organic solvents (THF, 1,4-Dioxane, ethanol and water) were carried out using a solid sample holder, a LifeSpec II spectrometer that is based on the TCSPC method, excitation at 375 nm using an Edinburgh diode laser with a repetition rate of 20 MHz, a time resolution of 30 ps, and a red-sensitive high-speed PMT detector (Hamamatsu, H5773-04). Emission decays were collected every 10 nm over the entire emission spectra of TTA-DFP COF with a dwell time of 10 s at each wavelength. The data were globally fitted to a 3-exponential model function convoluted with instrument response function (IRF) of ~30 ps, utilizing Least-Square Statistical Analysis (χ^2) and residual plot are used to assess the goodness of fit). The time-resolved data were specifically analyzed using Edinburgh

FAST software in which decay-associated spectra (DAS) were constructed from the extracted intensity-contribution fraction (f_i) calculated from the pre-exponential amplitudes (B_i), as follows:

$$I(t) = \sum_i B_i \exp(-t/\tau_i)$$

$$f_i = \frac{B_i \tau_i}{\sum_j B_j \tau_j}$$

Theoretical calculations by periodic density functional theory (DFT) were carried out using plane-wave calculations carried out using VASP¹ package considering spin-polarization and dipole corrections explicitly. Geometry optimization was performed using the model obtained in the structure determination. The total energies corresponding to the optimized geometries of all samples were calculated using the spin polarized version of the Perdew–Burke–Ernzerhof (PBE) implementation of the GGA exchange correlation functional.² The effect of the core electrons on the valence electron density was described by the project or augmented wave (PAW) method.³ In addition, the Heyd-Scuseria-Enzerhof hybrid functional (HSE06), with a mixing parameter of 0.225, was used to fit a more accurate energy gap. The cut-off for the kinetic energy of the plane-waves was set to 500 eV to ensure a total energy and force convergence better than 10⁻⁴ eV and 0.01 eV/Å³ respectively. The VESTA package v.39 was used to represent the charge density.⁴

Surface energy of the monolayer was calculated from DFT calculations of bulk and single layer nanosheet:

$$E_{Surf} = (E_{Single} - E_{Bulk})/3A$$

Where E_{Surf} is the surface energy and E_{Single} and E_{Bulk} are the energies from monolayer and bulk structures, A is de crystal surface and 3 is a factor to consider the number of layers including in the bulk structure.⁵

Theoretical optical properties were calculated using Time dependent Density Functional Theory (TD-DFT)⁶ implemented in the software Gaussian 09⁷ employing a PBE0 functional.² The standard 6–31G(d,p) basis set of double split valence plus polarization functions also on H atoms was chosen. Moreover, a fix number of 25 states were selected for a proper comparison between all configurations and models. Fluorescence images were obtained on an Olympus FV1000MPE confocal scanning microscope, images were taken with microscope power 60x.

S2: Synthetic Procedures

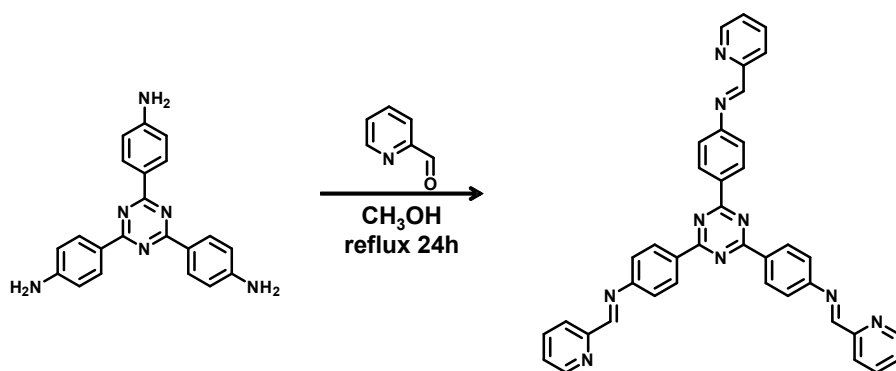
Synthesis of 2,6-diformylpyridine (DFP)

SeO₂ (4.25 g, 38.0 mmol) was added with stirring to a solution of 2,6-pyridinedimethanol (5.5 g, 39.4 mmol) in dioxane (100 mL) in a 250-mL round-bottom flask fitted with a condenser. The mixture was then stirred under reflux condition for 20 h before adding charcoal (4 scoops) to the reaction mixture. The mixture was heated for an additional 10 min and filtered hot through celite bed. The filter cake was washed with dioxane (3 × 50 mL) and CH₂Cl₂ (3 × 50 mL). After combining the filtrates, the solvents were removed under reduced pressure and the residue was purified by column chromatography [SiO₂: CH₂Cl₂] to afford DFP as a light pink solid. Yield: 77%; ¹H NMR (500 MHz, CDCl₃, 25 °C): δ 8.06 (t, 1H, *J* = 7.4 Hz, Ar-*H*), 8.17 (dd, 2H, *J* = 7.4 Hz, Ar-*H*), 10.16 (s, 2H, -CHO); ¹³C NMR (125 MHz, CDCl₃, 25 °C): δ 125.3, 138.4, 153.0, 192.3.

4,4',4''-(1,3,5-triazine-2,4,6-triyl)trianiline (TTA): The triamine (TTA) was synthesized according to the published procedure with no modifications.⁸

Synthesis of TTA-DFP COF under Microwave condition: A microwave reaction vessel (25 mL), was charged with 1,3,5-tris(4-aminophenyl)benzene (21 mg, 0.06 mmol, 2 equiv) and 2,6-pyridinedicarboxaldehyde (12 mg, 0.09 mmol, 3 equiv). Anhydrous 1,4-dioxane (3.0 mL) was added, and the resulting mixture was sonicated for 1 min. An aqueous solution of acetic acid (0.5 mL, 3.0 M) was added, resulting in immediate formation of a yellow precipitate. The resulting mixture was stirred under microwave irradiation of 2.45 GHz at 100 °C for 30 min and subsequently cooled to room temperature. The precipitate was collected by centrifugation and washed with anhydrous ethanol five times and with water twice. The powder was dried at 120 °C under vacuum overnight to yield the yellow colored product.

Synthesis of 4,4',4''-(1,3,5-triazine-2,4,6-triyl)triimino-2-pyridine TTA monomer.



Pyridine-2-carbaldehyde (0.235, 2.46 mmol) and 4,4',4''-(1,3,5-triazine-2,4,6-triyl)trianiline (0.250 g, 0.705 mmol) in anhydrous methanol was refluxed in sealed tube for 20h. After the reaction completion, the formed precipitate was filtered in hot condition, recrystallized from hot ethanolic solution and dried in vacuum overnight to give a pale yellow powder, yield 82 %; ¹H

NMR (500 MHz, CDCl₃, 25 °C): δ 7.43-7.49 (m, 9H, Ar-H), 7.87-7.90 (m, 3H, Ar-H), 8.28 (d, 3H, $J = 7.9$ Hz, Ar-H), 8.72 (s, 3H, CH=N), 8.78-8.79 (m, 3H, Ar-H), 8.88-8.90 (m, 6H, Ar-H); ¹³C NMR (125 MHz, CDCl₃, 25 °C): δ 121.3, 122.2, 125.5, 130.3, 134.5, 136.8, 149.9, 154.4, 154.9, 161.8, 170.1.

Liquid Phase Exfoliation Process:

2 mg of TTA-DFP COFs were suspended into 10 mL of pure water then exposed to liquid phase ultra-sonication with a frequency of 20 kHz. We obtained a homogeneous dispersion of TTA-DFP CONs. Solution pictures before and after exfoliation are displayed in Figures S5 and S10.

S3. Fourier Transform Infrared (FTIR) Spectroscopy of the Synthesized TTA-DFP COF/CONs Materials and their Precursors

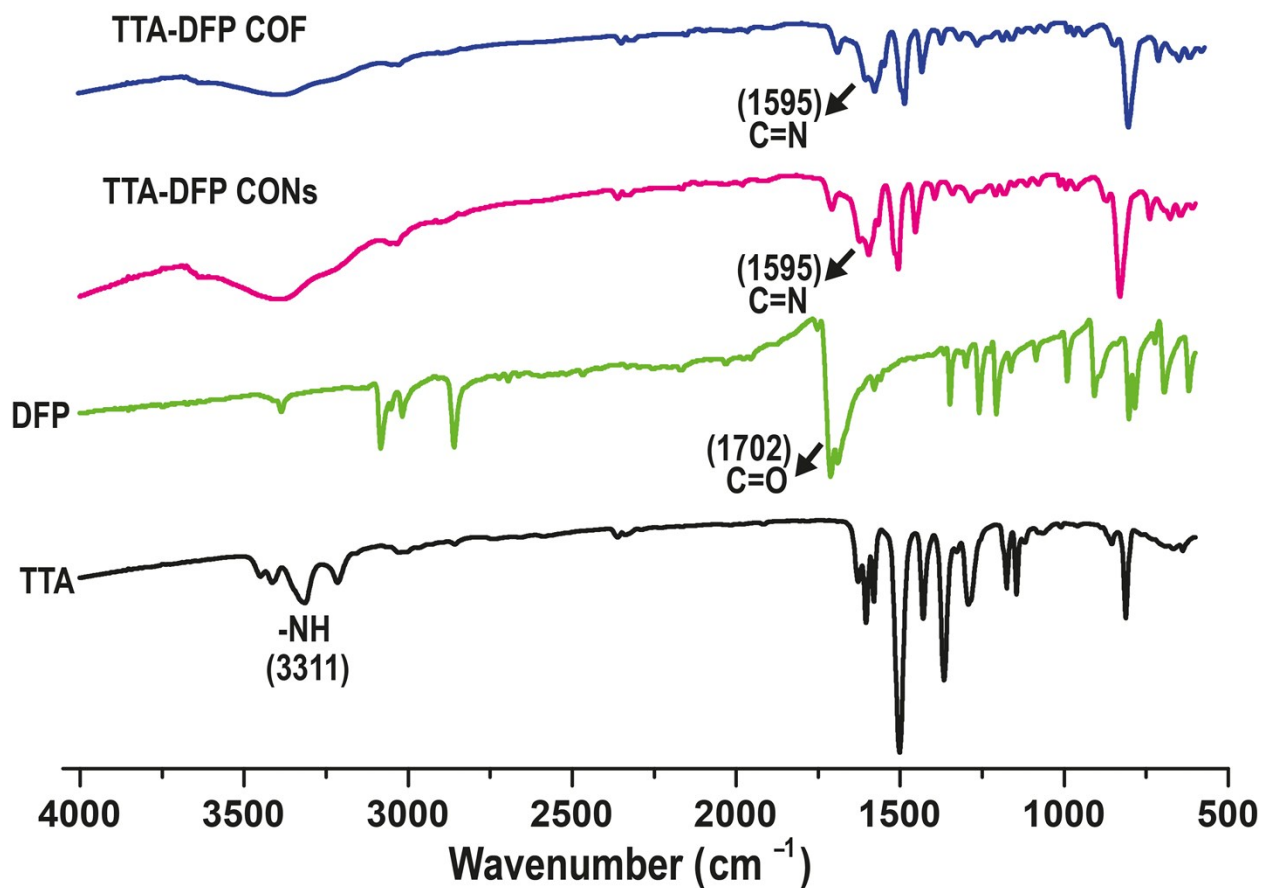


Figure S1: Stacked FTIR spectra of TTA-DFP COFs/CONs and their precursors, 2,6-diformylpyridine (DFP) and 4,4',4''-(1,3,5-triazine-2,4,6-triyl)trianiline (TTA).

S4: Thermogravimetric Analyses of TTA-DFP COF and TTA-DFP CONs Materials

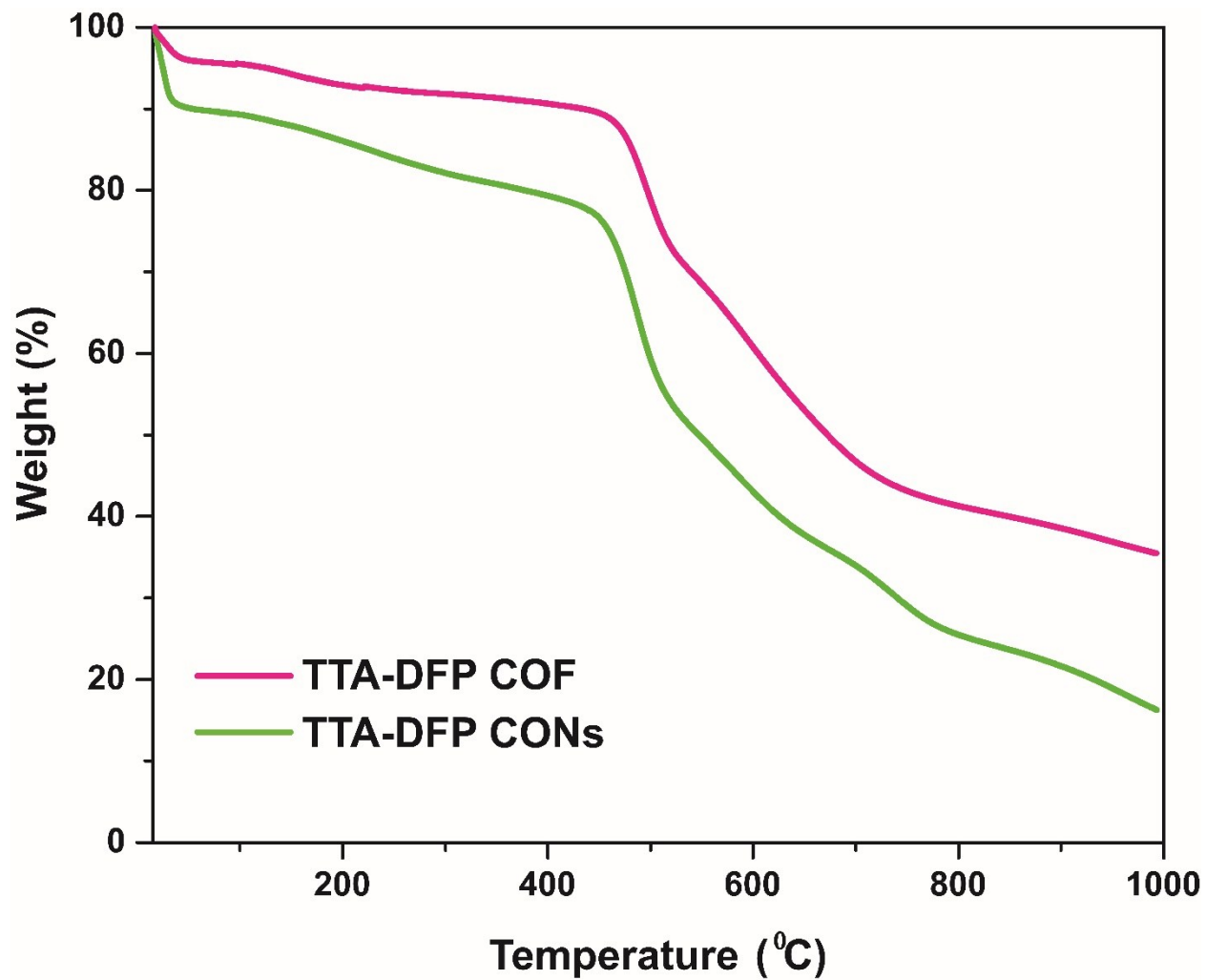


Figure S2: TGA analysis of TTA-DFP COFs/CONs.

S5: Pore Size Distribution of TTA-DFP COF

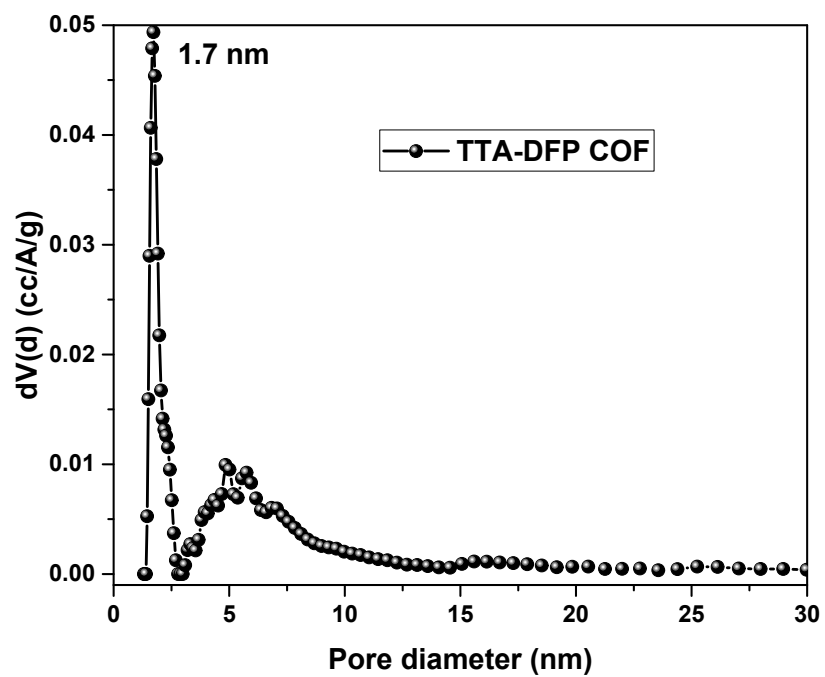


Figure S3: Pore size distribution analysis of TTA-DFP COF.

S6: HRTEM and AFM Analysis of TTA-DFP COF and TTA-DFP CONs

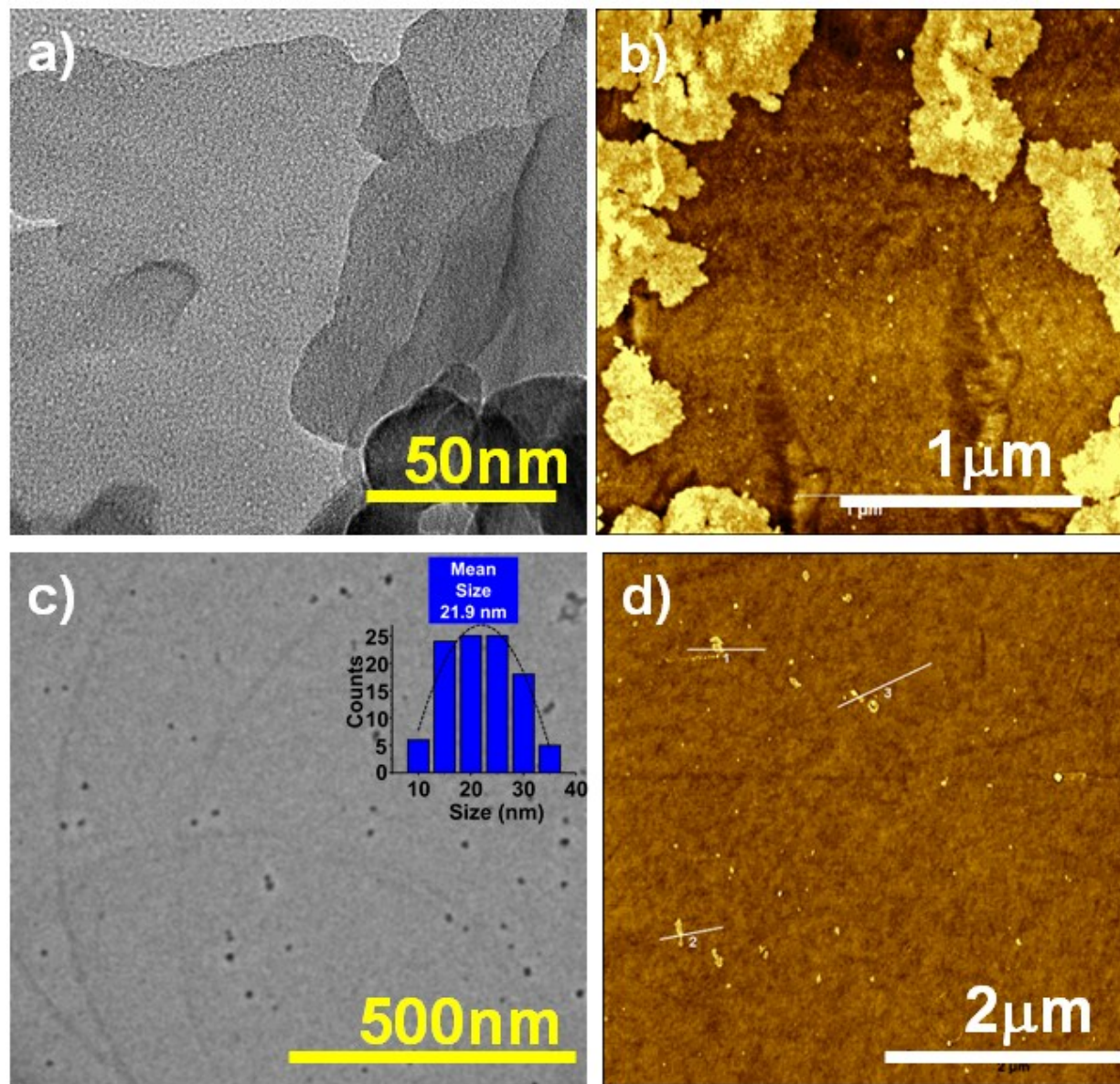


Figure S4: HRTEM and AFM images of TTA-DFP COF (a-b) and TTA-DFP CONs (c-d).

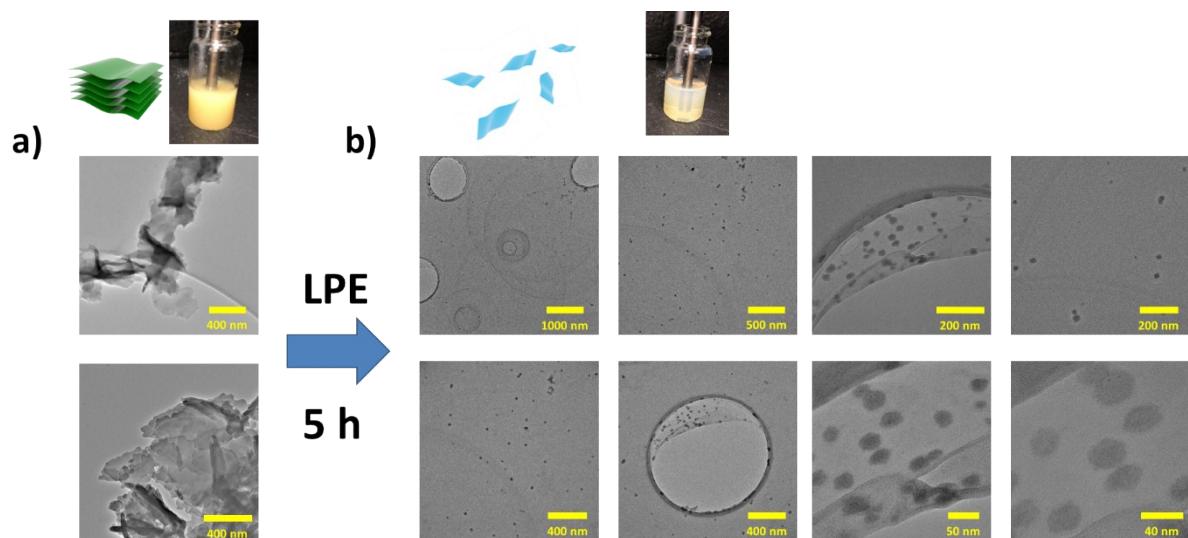


Figure S5: TEM images of a) TTA-DFP COFs and b) TTA-DFP CONs. After 5 hours of ultrasonication in water, exfoliation into nanosheets is achieved and a homogeneous dispersion of TTA-DFP CONs is obtained showing that most of the COFs were exfoliated into CONs with limited aggregation. Top: solution pictures before (left) and after (right) exfoliation.

S7: AFM Height Profiles of TTA-DFP COF and TTA-DFP CONs

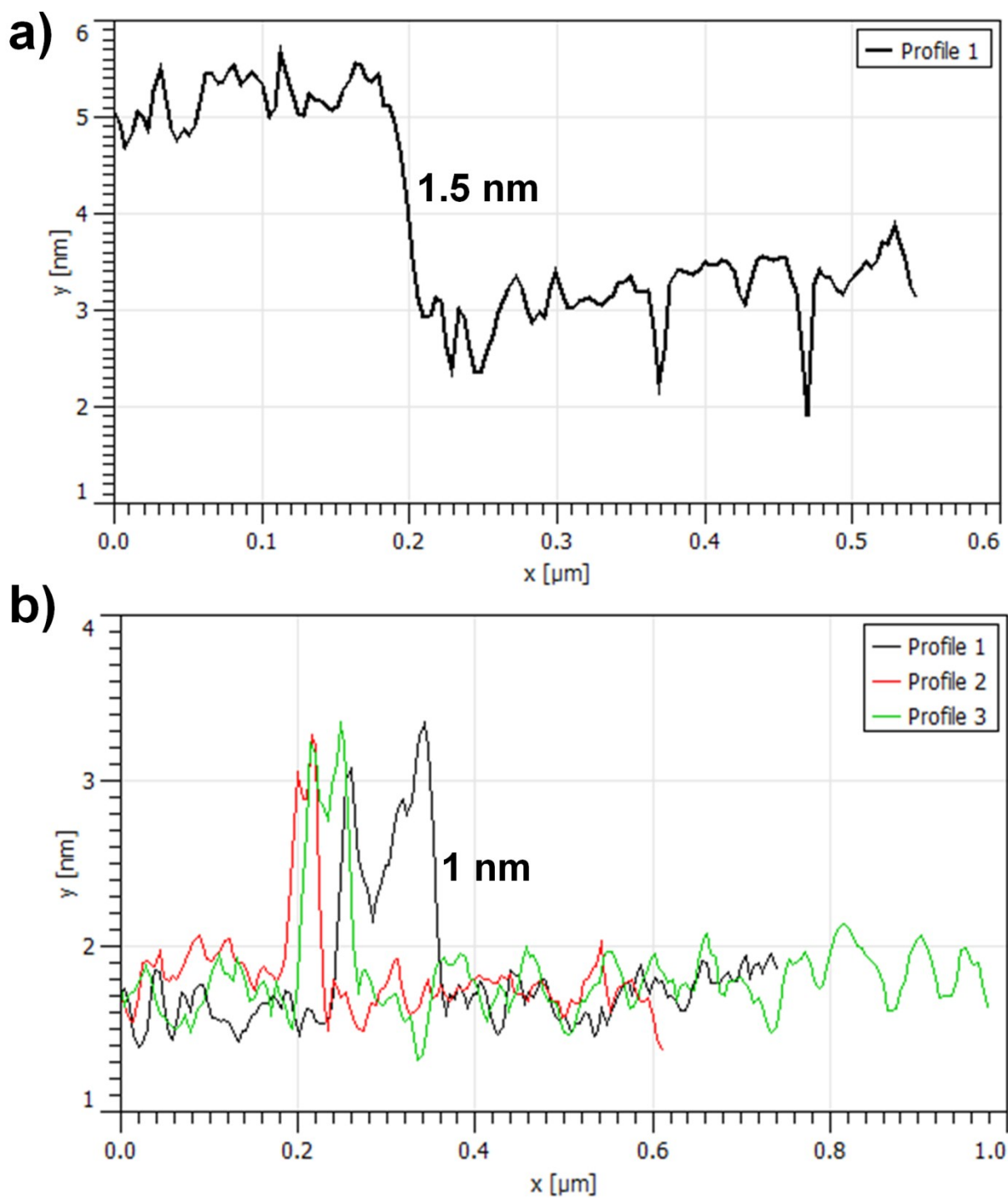


Figure S6: AFM height profiles of a) TTA-DFP COF and b) TTA-DFP CONs.

S8: Room Temperature PXRD Patterns of TTA-DFP CONs

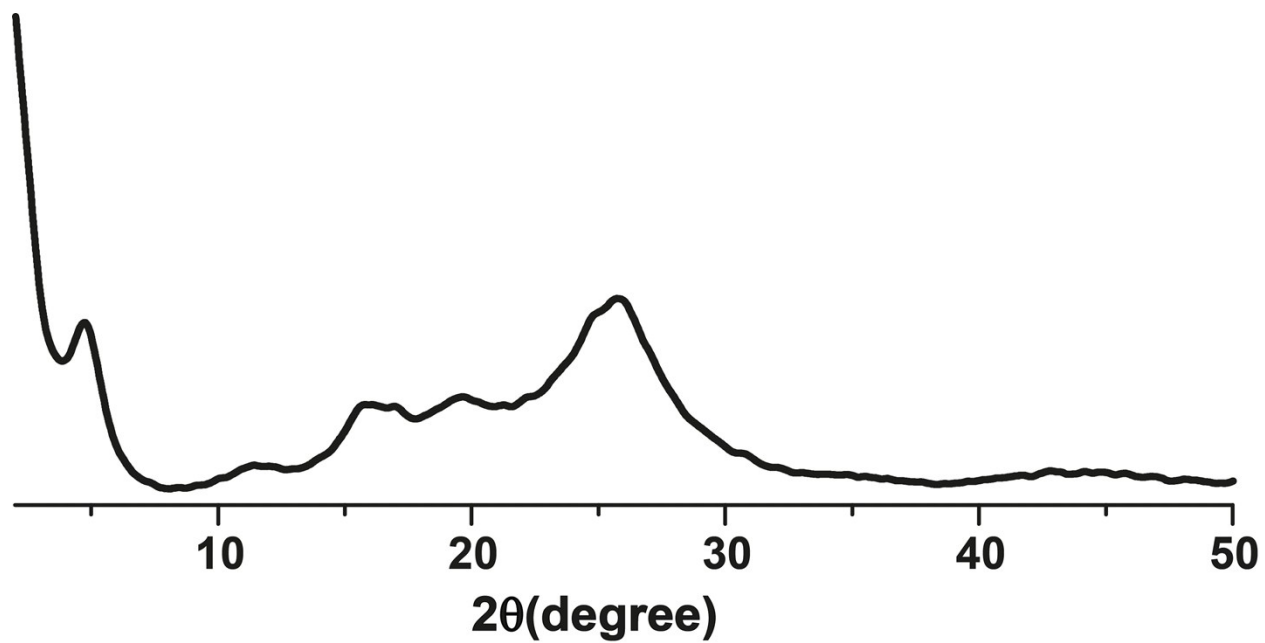


Figure S7: Room temperature PXRD pattern of TTA-DFP CONs.

S9: Dynamic Light Scattering (DLS) Characterization

DLS measurements were carried out on a Zetasizer Nano-ZS (Malvern Instruments) to determine the hydrodynamic diameter of the TTA-DFP CONs.

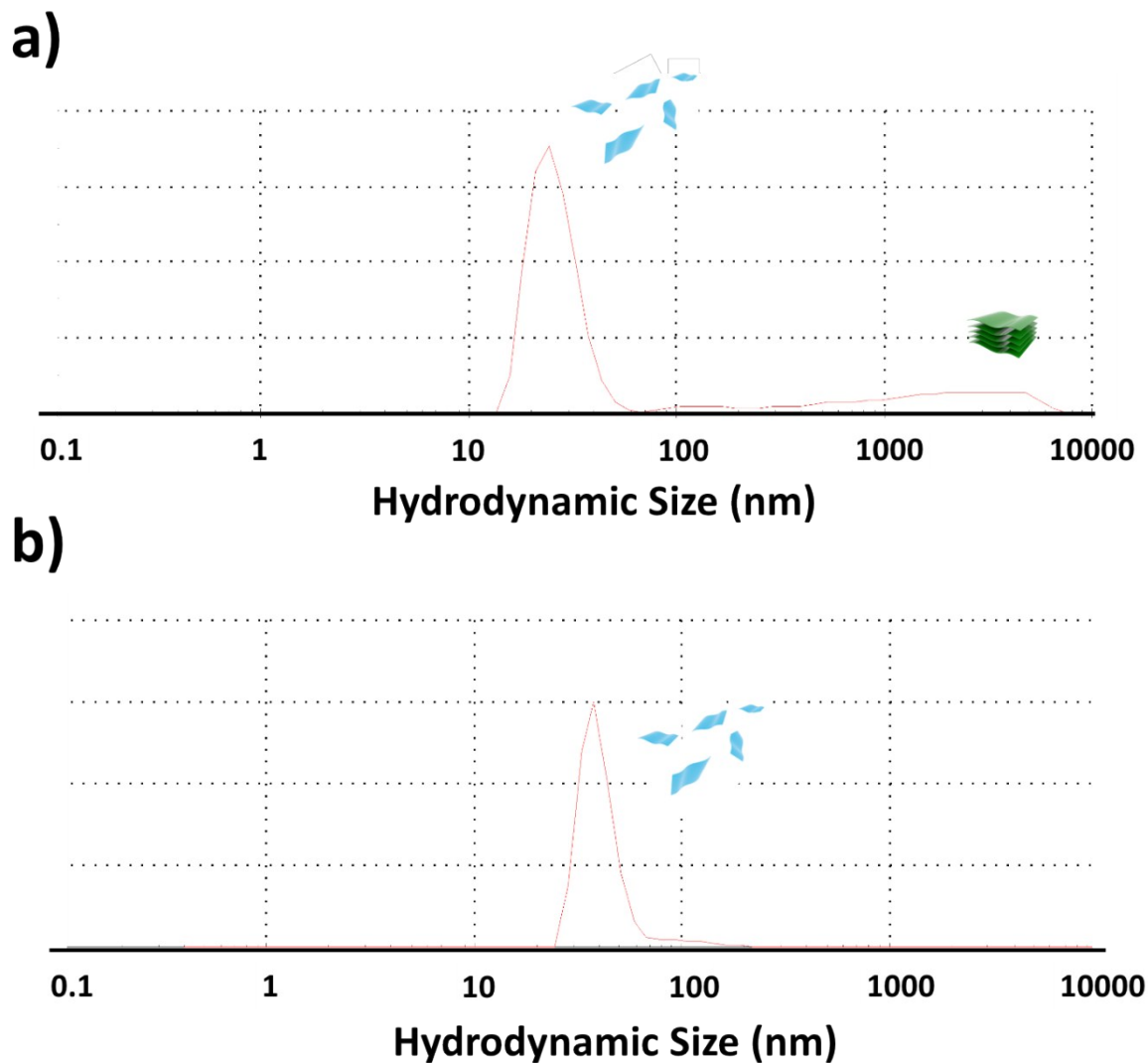


Figure S8: Hydrodynamic diameter of TTA-DFP CONs in water at pH 7.4 before a) and after b) filtration to remove non-exfoliated COFs.

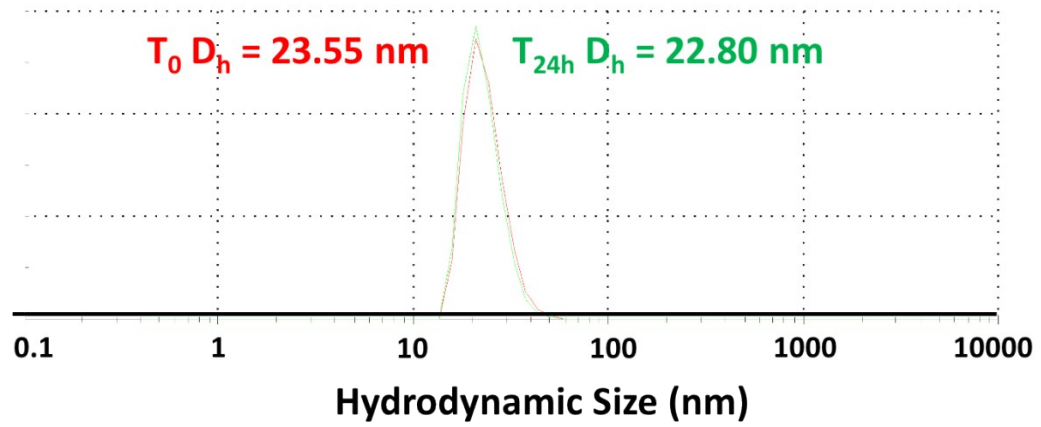


Figure S9: Hydrodynamic diameter of TTA-DFP CONs in fetal bovine serum (FBS) at $t = 0\text{h}$ and after 24 hours.

S9: Luminescent Study of TTA-DFP COF/CONs and TTA-DFP COF Monomer

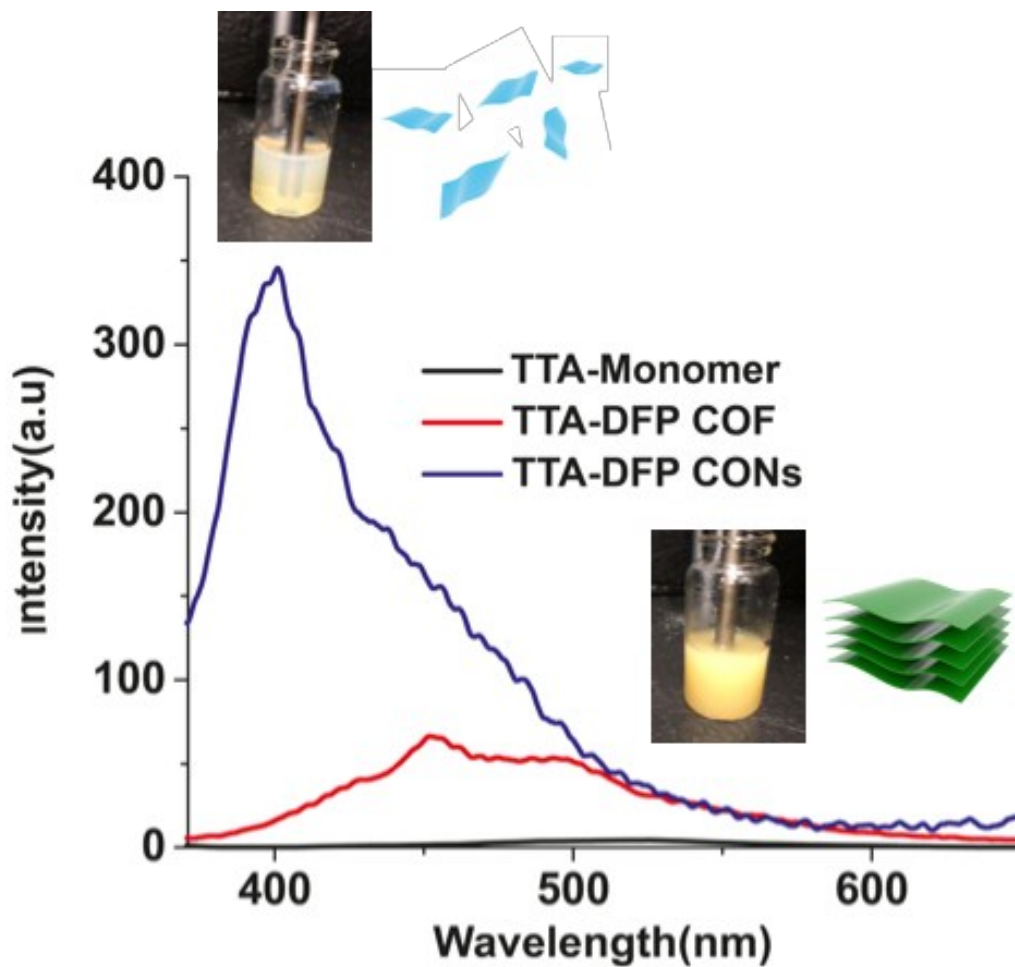


Figure S10: Photoluminescent spectra of TTA-DFP monomer (black), TTA-DFP COF (red) and TTA-DFP CONs (blue), in water at room temperature with $\lambda_{ex} = 375$ nm. The monomer did not show any luminescent property compared to the TTA-DFP COF/CONs. Pictures of the same solution before and after 5 hours of ultra-sonication.

S10: Plane Wave Density Functional Theory (PW-DFT) Analysis

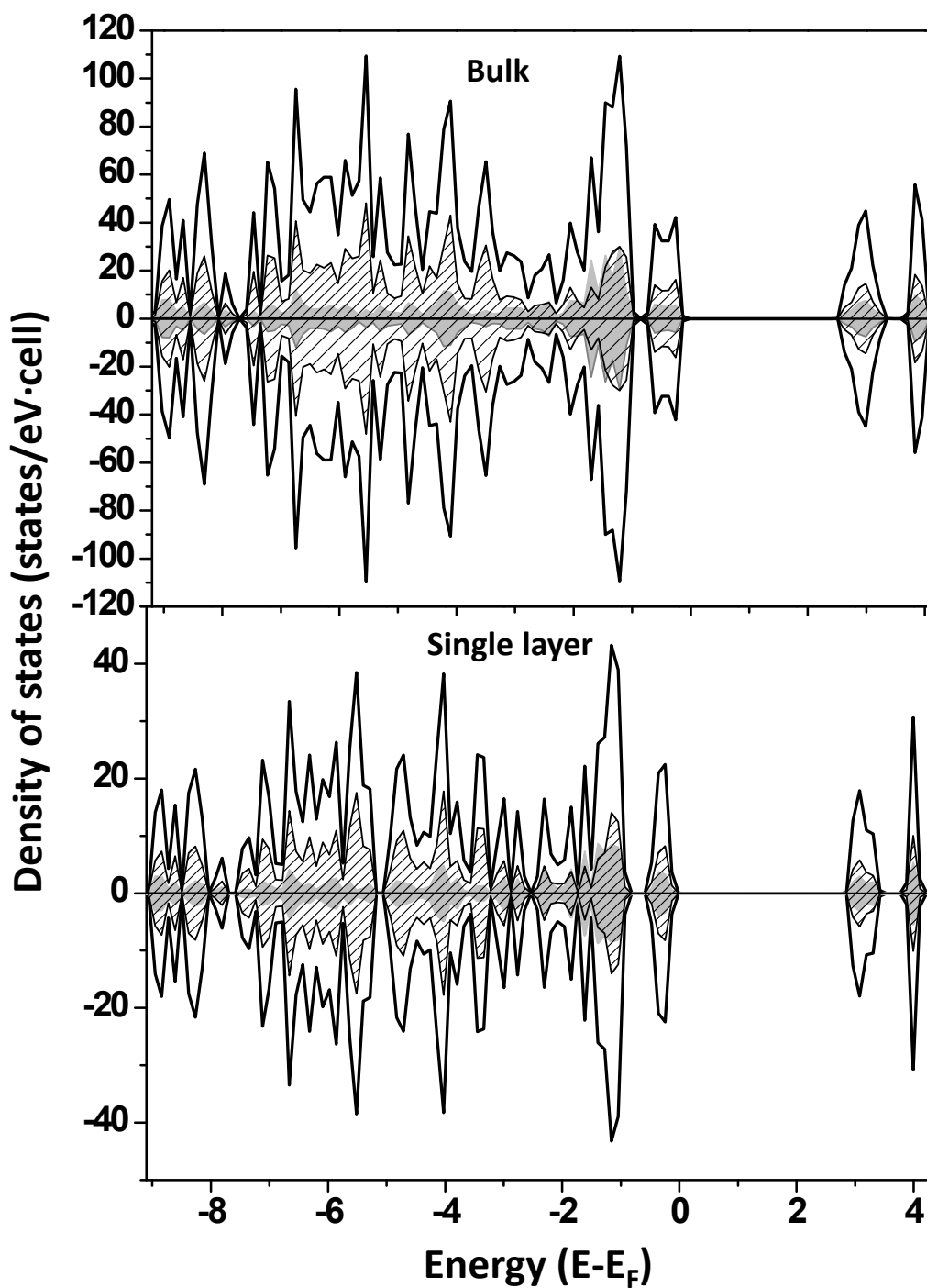


Figure S11: Density of state (DOS) calculations in bulk phase and single layer. DOS study were carried out by using plane-wave calculations carried out using VASP1 package considering spin-polarization and dipole corrections explicitly.

S11: Band Gap Calculations for UV-Vis Spectra

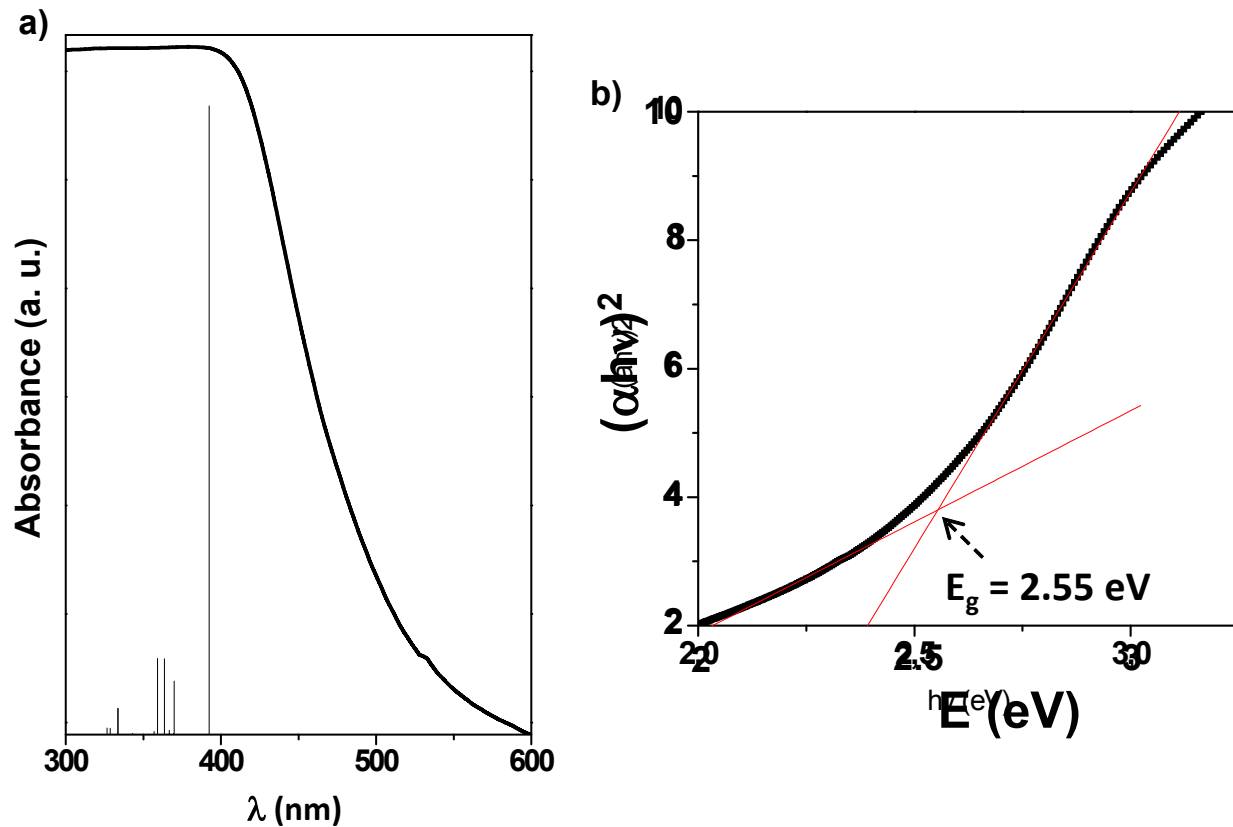


Figure S12: a) Solid state UV-Vis spectrum of TTA-DFP COF and time dependent density functional theory, TD-DFT (6-311G**) calculated excitation energies (vertical bars), b) Tauc plot for the calculation of optical band gap. Band gap calculation using UV-Vis (tauc plot) is calculated as the edge of the absorption band.

S12: The frontier molecular orbital distributions of TTA-DFP CONs fragment by DFT calculations

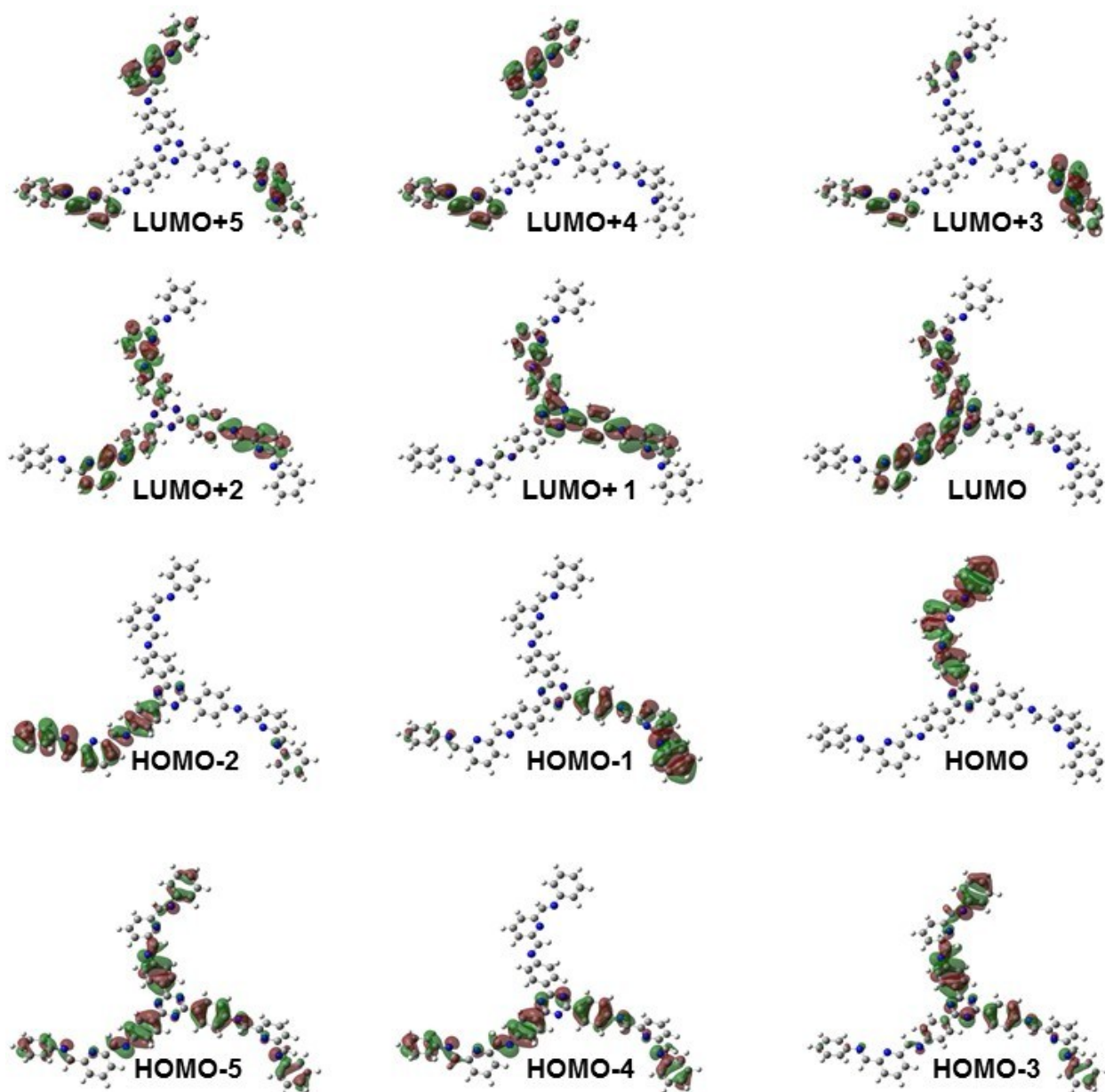


Figure S13: HOMO-LUMO energy diagram of TTA-DFP CONs obtained from time dependent density functional theory, TD-DFT (6-311G**) calculations.

S13: Biological Studies

13.1. Cell culture

Cervical cancer cells (HeLa, ATCC No. CCL-2) were cultured at 37 °C under condition of 5 % CO₂ in Dulbecco's Modified Eagle's medium (DMEM) supplemented with 10 % fetal bovine serum (FBS) and 1 % penicillin/streptomycin.

13.2. In vitro cellular uptake kinetic

HeLa cells were seeded on sterile cover-slips in a 6-well plate ($\sim 50,000$ cell.mL⁻¹) and incubated for 24 hours. After 24 hours, the medium was replaced with fresh DMEM (control), or TTA-DFP CONs (100 $\mu\text{g.mL}^{-1}$) and the cells were incubated at 37 °C, 5 % CO₂ for 15 minutes up to 24 hours, followed by three cycles of PBS washing to remove the nanosheets that did not penetrate the cells. Then, for each experiment, the cells were fixed with formaldehyde solution (3.7 %) for 10 min followed by washing thrice with PBS. The cells were kept for 5 min in the PBS during washing cycles. The cover-slips were then fixed onto a microscope slide.

The intracellular internalization of TTA-DFP CONs was observed using fluorescence microscopy (Leica DMI6000B) in HeLa cells (360 nm).

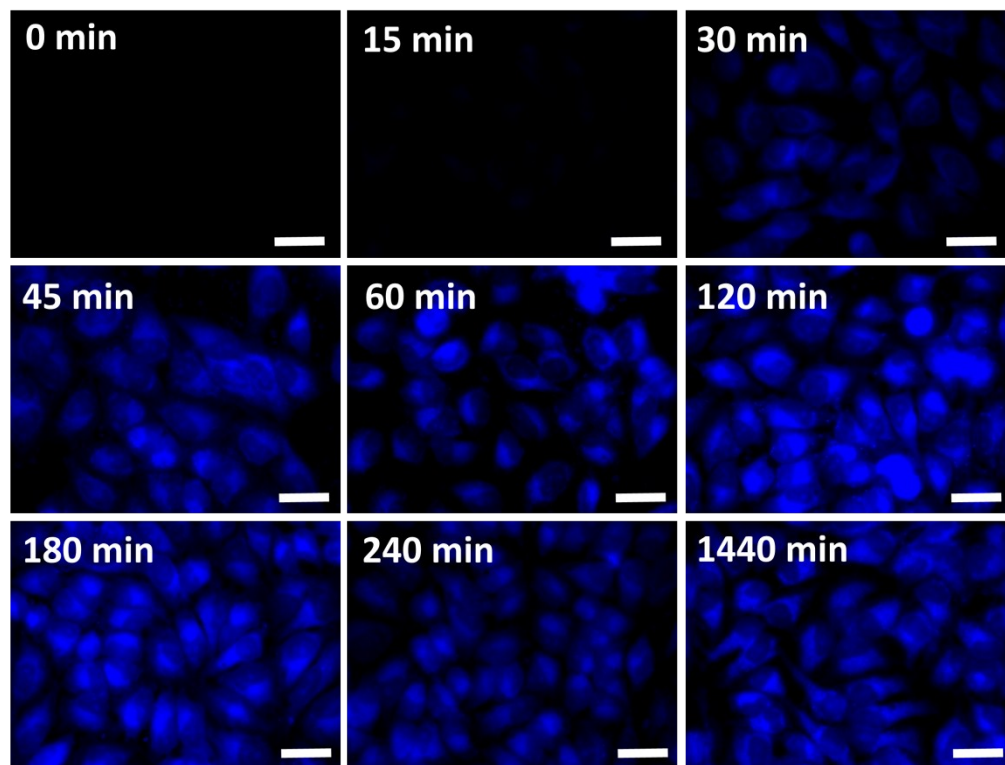


Figure S14: Fluorescence images of HeLa cells incubated with the exfoliated TTA-DFP CONs (100 $\mu\text{g.mL}^{-1}$) for 0, 15, 30, 45, 60, 120, 180, 240 and 1440 minutes; blue channel ($\lambda_{\text{ex}} = 360$ nm). Scale bar (10 μm).

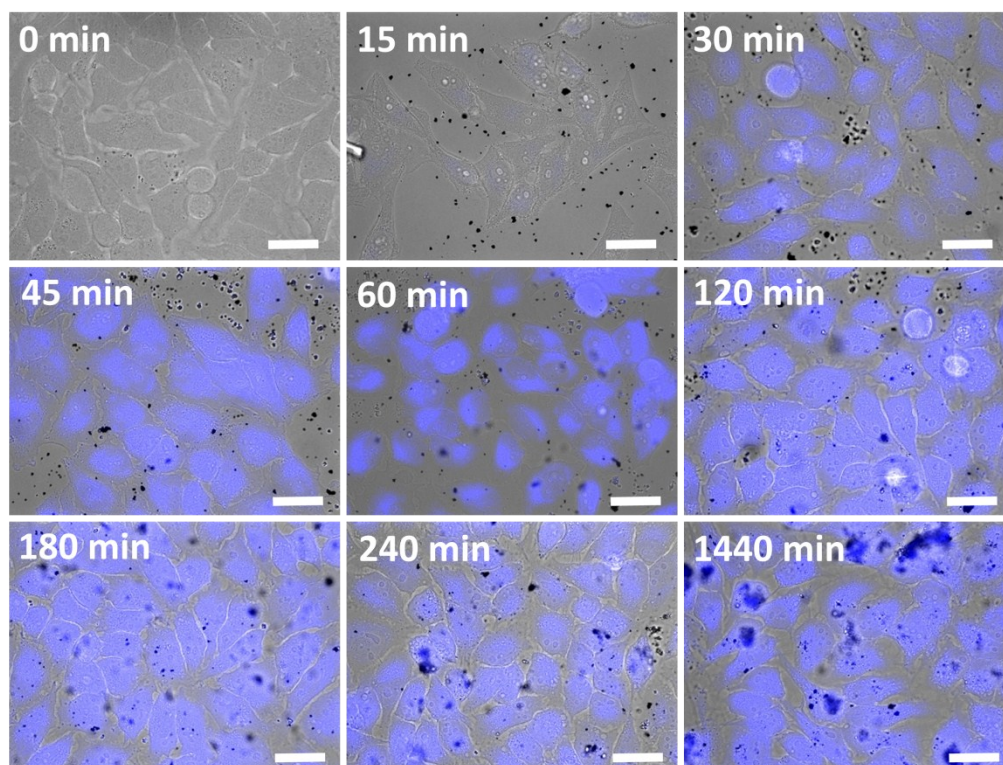


Figure S15: Overlay of fluorescence and bright field images of HeLa cells incubated with the exfoliated TTA-DFP CONs ($100 \mu\text{g}\cdot\text{mL}^{-1}$) for 0, 15, 30, 45, 60, 120, 180, 240 and 1440 minutes; blue channel ($\lambda_{\text{ex}} = 360 \text{ nm}$). Scale bar ($10 \mu\text{m}$).

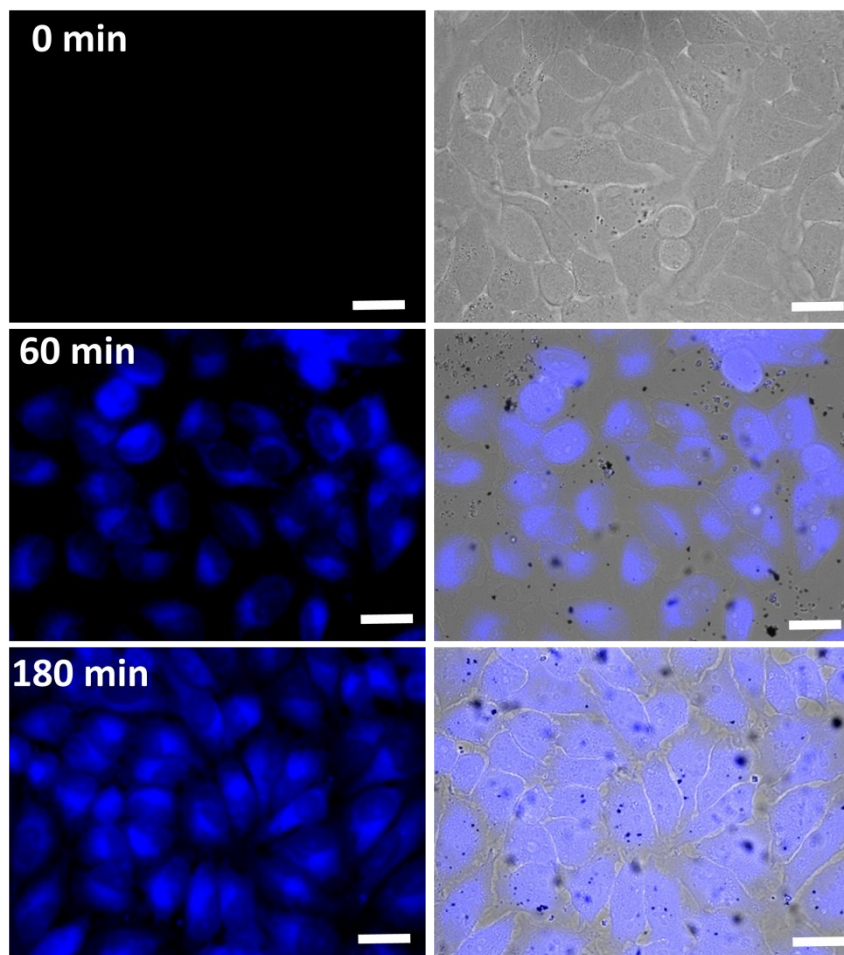


Figure S16: Fluorescence and bright field images of HeLa cells incubated with the exfoliated TTA-DFP CONs ($100 \mu\text{g}\cdot\text{mL}^{-1}$) for 0, 60, 180 minutes; blue channel ($\lambda_{\text{ex}} = 360 \text{ nm}$). Scale bar ($10 \mu\text{m}$).

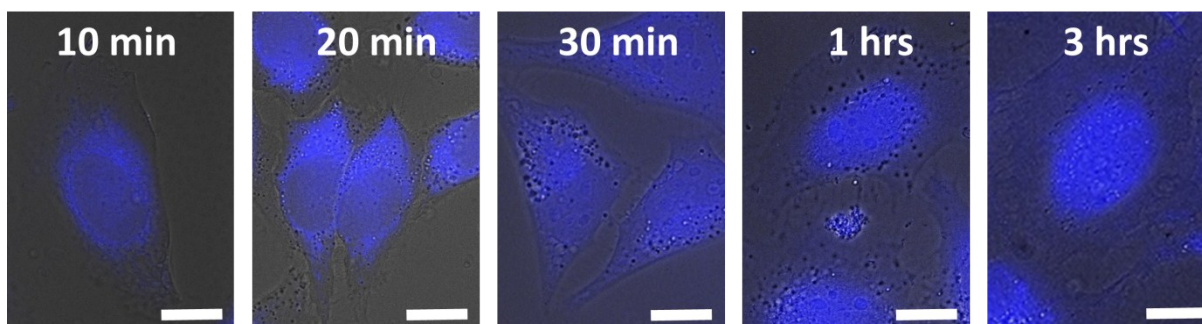


Figure S17: Overlay of fluorescence and bright field images of HeLa cells incubated with the exfoliated TTA-DFP CONs ($150 \mu\text{g}\cdot\text{mL}^{-1}$) for 10, 20, 30, and 180 minutes; blue channel ($\lambda_{\text{ex}} = 360 \text{ nm}$). Scale bar ($5 \mu\text{m}$).

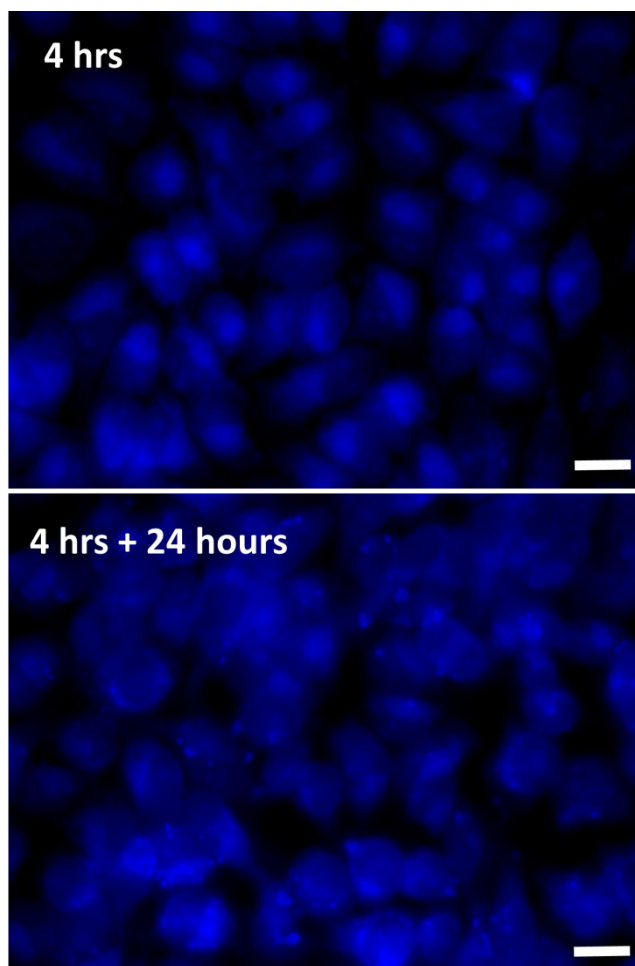


Figure S18: Fluorescence images of HeLa cells incubated with the exfoliated TTA-DFP CONs ($100 \mu\text{g}\cdot\text{mL}^{-1}$) for either 4 hours or 4 h and then subsequently incubated for 24 h with the fresh media without TTA-DFP CONs; blue channel ($\lambda_{\text{ex}} = 360 \text{ nm}$). Scale bar (10 μm).

13.2. In vitro cellular localization

HeLa cells were seeded on sterile cover-slips in a 6-well plate ($\sim 50,000 \text{ cell}\cdot\text{mL}^{-1}$) and incubated for 24 hours. After 24 hours, the medium was replaced with fresh DMEM (control), or TTA-DFP CONs ($50 \mu\text{g}\cdot\text{mL}^{-1}$) and the cells were incubated at $37 \text{ }^\circ\text{C}$, 5 \% CO_2 for 4 h, followed by three cycles of PBS washing to remove the nanosheets that did not penetrate the cells, and fresh DMEM was replaced. The cells were stained with organelles markers to understand the internalization of TTA-DFP CONs from cytosol to the inside of the nucleus. Cells were incubated for 30 min either with NucRed® Live 647 ReadyProbes® Reagent (labelling nucleus), ActinRed™ 555 ReadyProbes™ Reagent (labeling cytoplasm) and CellMask™ Deep Red (labeling membrane), followed by three cycles of PBS washing. Then, for each experiment, the cells were fixed with formaldehyde solution (3.7 %) for 10 min followed by washing thrice with PBS. The cells were kept for 5 min in the PBS during washing cycles. ProLong Live Antifade Reagent was added to

suppress photo-bleaching and preserves the fluorescent signals. The cover-slips was then fixed onto a microscope slide.

The intracellular internalization of TTA-DFP CONs was observed using confocal microscopy (Olympus FV1000MPE) measuring the fluorescence signal of the nanosheets (405 nm) in HeLa cells as well as the fluorescence emission from the 3 organelle markers labeling the plasmic membrane (633 nm), the cytoplasm (560 nm) as well as the nucleus (633 nm).

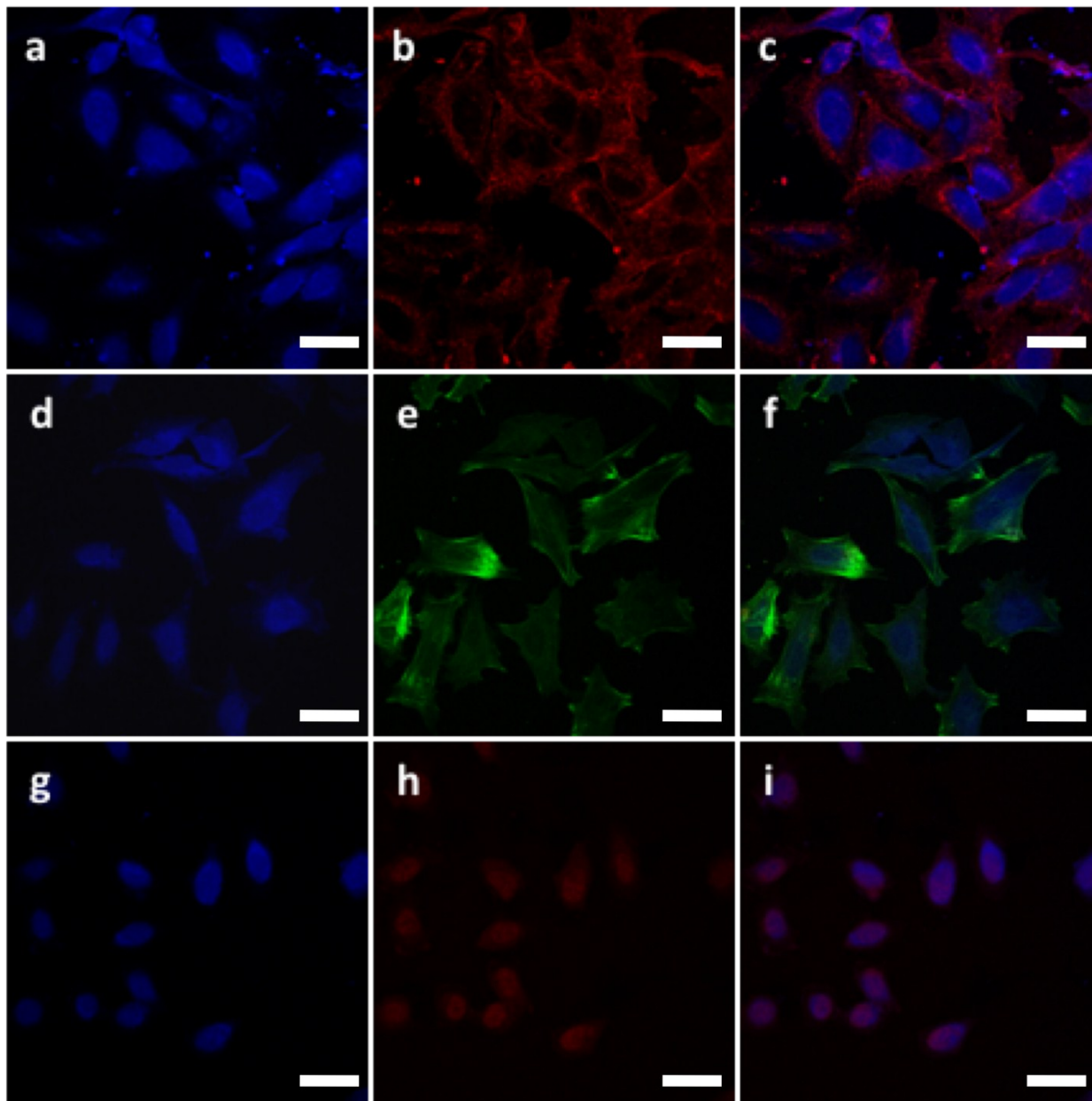


Figure S19: Confocal images of HeLa cells incubated for 4 hours with the exfoliated TTA-DFP CONs (50 $\mu\text{g}/\text{mL}$) and a, b, c) a plasmic membrane marker, d, e, f) an actin marker and g, h, i) a nucleus marker. a, d, g) blue channel ($\lambda_{\text{ex}} = 405 \text{ nm}$); c, h) red channel ($\lambda_{\text{ex}} = 633 \text{ nm}$); e) green

channel ($\lambda_{\text{ex}} = 561 \text{ nm}$). c, f, i) overlay of a and b, d and e, and g and h, respectively, Scale bar ($10 \mu\text{m}$).

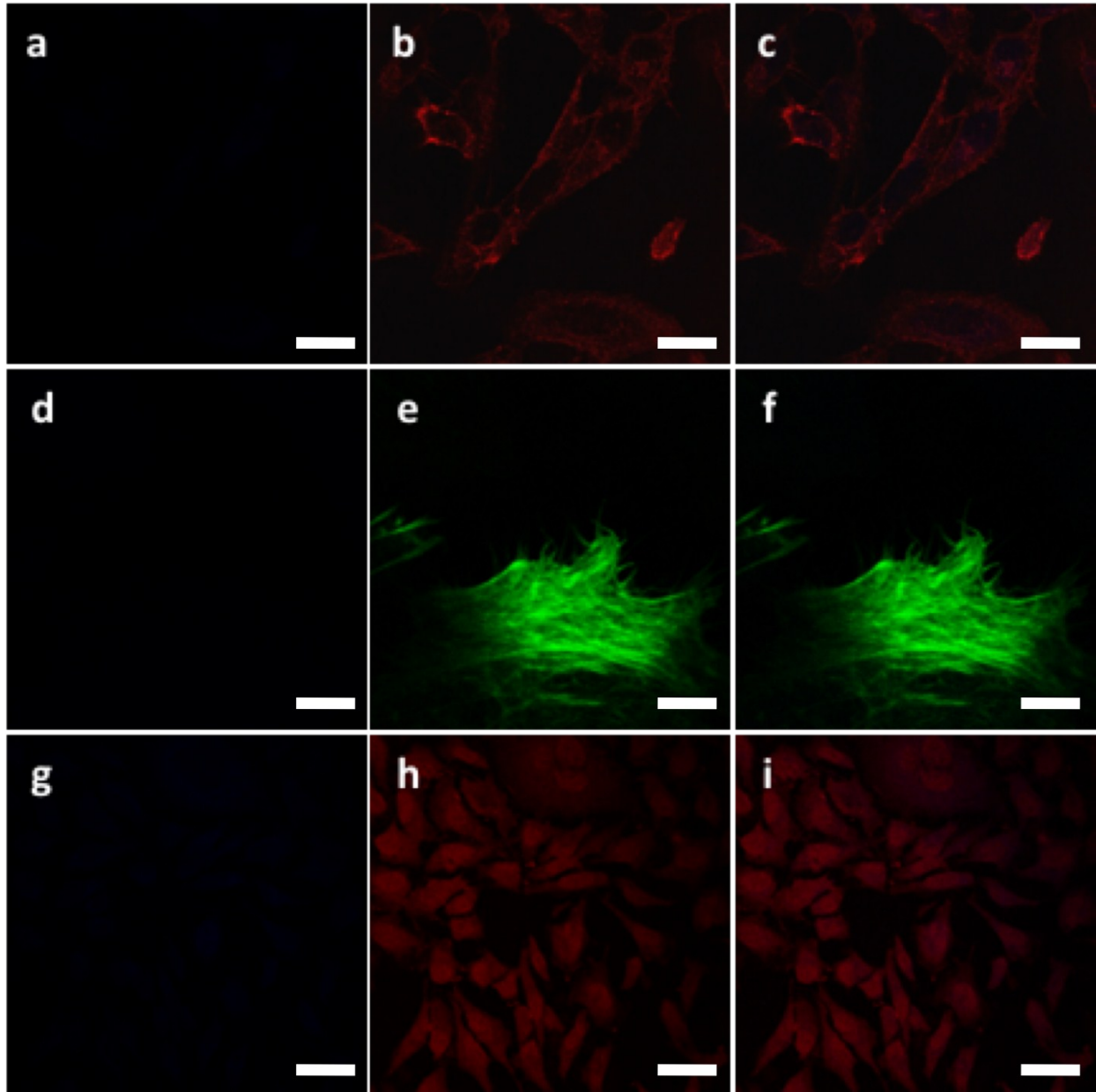


Figure S20: Confocal images of HeLa cells incubated 4 hours with no additives and a, b, c) a plasmic membrane marker, d, e, f) an actin marker and g, h, i) a nucleus marker. a, d, g) blue channel ($\lambda_{\text{ex}} = 405 \text{ nm}$); c, h) red channel ($\lambda_{\text{ex}} = 633 \text{ nm}$); e) green channel ($\lambda_{\text{ex}} = 561 \text{ nm}$). c, f, i) overlay of a and b, d and e, and g and h, respectively, Scale bar ($20 \mu\text{m}$).

13.3. Mechanism of cellular internalization HeLa cells

HeLa cells were seeded on sterile cover-slips in a 6-well plate ($\sim 50,000$ cell.mL⁻¹) and incubated for 24 hours. To examine the different internalization pathways, HeLa cells were pre-incubated with chlorpromazine (5 μ M), filipin III (5 μ M) or amiloride (10 μ M) in cell culture medium for 30 min at 37 °C, before the incubation with TTA-DFP CONs (50 μ g.mL⁻¹) and the cells were incubated at 37 °C, 5 % CO₂ for 4 h, followed by three cycles of PBS washing to remove the nanosheets that did not penetrate the cells. Control cells were incubated with TTA-DFP CONs (50 μ g.mL⁻¹) without any pre-treatment. Then, for each experiment, the cells were fixed with formaldehyde solution (3.7 %) for 10 min followed by washing thrice with PBS. The cells were kept for 5 min in the PBS during washing cycles. The cover-slips were then fixed onto a microscope slide.

The effect of the inhibitors on TTA-DFP CONs cell uptake was calculated by measuring the relative fluorescence intensity in cells and compared to cells treated with TTA-DFP CONs without any pre-treatment using fluorescence microscopy (Leica DMI6000B) in HeLa cells (360 nm).

Endocytic Inhibitor	Pathway inhibited	Concentration (μ M)
Chlorpromazin	Clathrin-mediated endocytosis	5
Filipin	Clathrin-independant endocytosis	5
Amiloride	Macropinocytosis	10

Table S1: Concentrations of endocytic inhibitors used in this study.

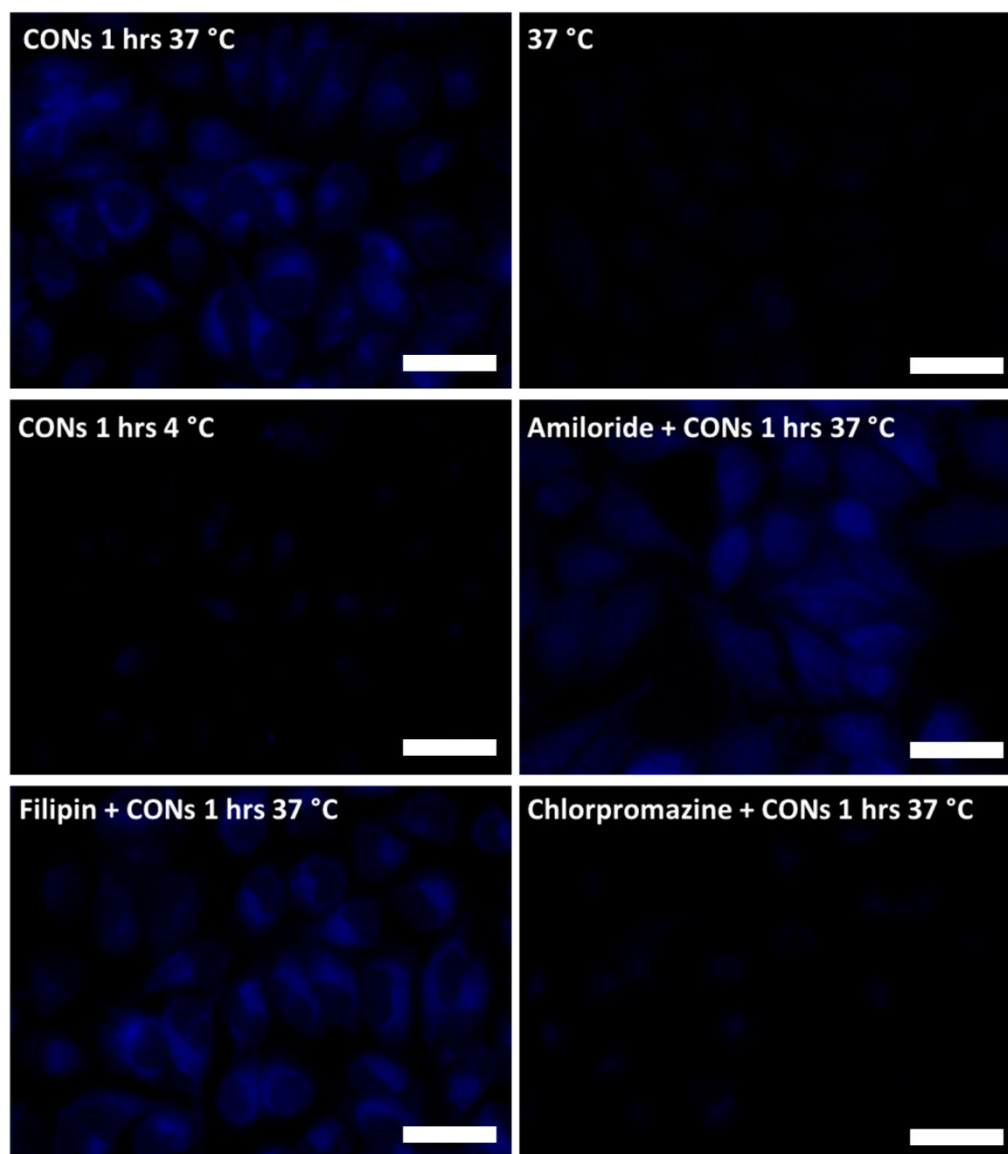


Figure S21: Fluorescence images of HeLa cells incubated for 4 hours with the exfoliated TTA-DFP CONs ($50 \mu\text{g.mL}^{-1}$) at $37 \text{ }^\circ\text{C}$, $4 \text{ }^\circ\text{C}$, and with pre-treatment with Chlorpromazin, Filipin and Amiloride at $37 \text{ }^\circ\text{C}$; blue channel ($\lambda_{\text{ex}} = 360 \text{ nm}$). Scale bar ($20 \mu\text{m}$).

16.3. *In vitro* cell viability assay

Effect of TTA-DFP CONs, DFP and TTA on HeLa cell viability was assessed using CellTiter-Blue® Cell Viability assay (CTB, Promega). The assay measures the metabolic reduction of a non-fluorescent compound, resazurin, into a fluorescent product, resofurin, in living cells. As non-viable cells rapidly lose their metabolic activity, the amount of the resofurin product can be used to estimate the number of viable cells following treatment. Once produced, resofurin is released

from living cells into the surrounding medium. Thus, the fluorescence intensity of the medium is proportional to the number of viable cells present.

96-well plates were seeded with cells (~5,000 cells per well in 100 μL of DMEM) and incubated at 37 $^{\circ}\text{C}$ for 24 hours. The medium was removed and replaced with fresh DMEM (control) or various concentrations of TTA-DFP CONs (up to 500 $\mu\text{g}\cdot\text{mL}^{-1}$), as well as TTA and DFP (up to 250 $\mu\text{g}\cdot\text{mL}^{-1}$) and incubated at 37 $^{\circ}\text{C}$ for 48 hours. Thereafter, cells were washed with PBS and incubated with 20 μL of CTB per well for 6 hours at 37 $^{\circ}\text{C}$. The fluorescence of the resofurin product ($\lambda_{\text{ex/em}}$ 560/620) was measured. Untreated wells were used as control.

The percentage of cell viability and inhibition were calculated using the following formula:

$$\text{Viability (\%)} = [(F_{\text{treated}} - F_{\text{blank}}) / (F_{\text{control}} - F_{\text{blank}})] \times 100$$

$$\text{Inhibition (\%)} = 100 - \text{viability (\%)}$$

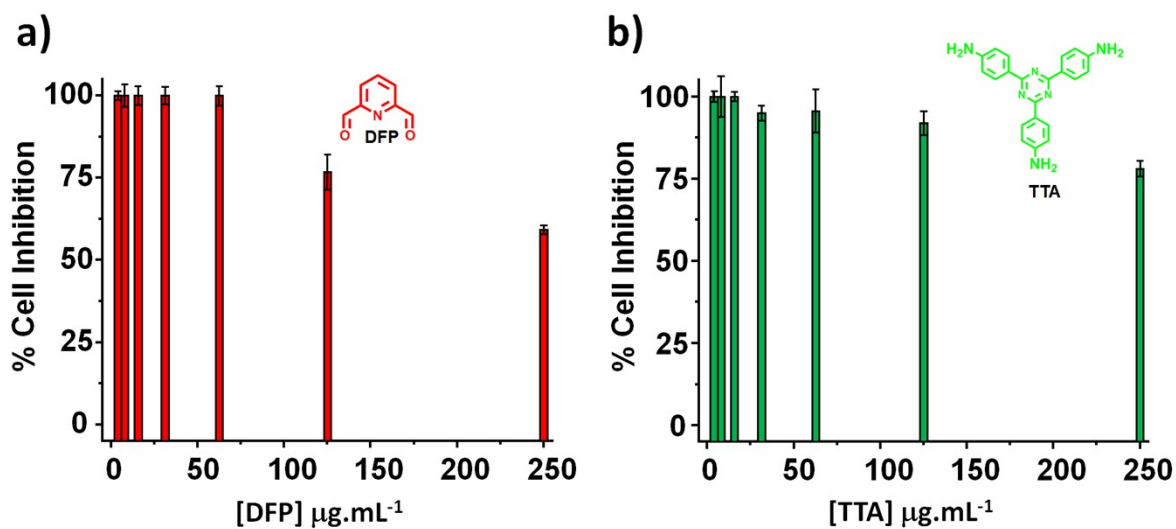


Figure S22: Viability assessment of HeLa cells after 48 h incubation with increasing concentrations of a) DFP and b) TTA up to 250 $\mu\text{g}\cdot\text{mL}^{-1}$.

	Emission	Membrane permeability	Dead/live cell staining	Cytotoxicity
DAPI	Blue	<i>slightly permeable</i>	Dead cell	yes
Hoechst 33258	Blue	<i>membrane permeable unmediated diffusion transport mechanism</i> ^{9,10}	Live and dead cell	Yes and no
TTA-DFP CONs	Blue	<i>membrane permeable Clathrine mediated endocytosis</i> -	Live cell	no

Table S2: Comparison of TTA-DFP CONs with blue fluorescent DNA dyes commercially available.

References

1. a) G. Kresse and J. Furthmüller, *Comput. Mater. Sci.*, 1996, **6**, 15-50.; b) G. Kresse and J. Hafner, *Phys. Rev. B*, 1993, **47**, 558–561.
2. a) J. P. Perdew, K. Burke and M. Ernzerhof, *Phys. Rev. Lett.*, 1996, **77**, 3865–3868; b) J. P. Perdew, K. Burke and M. Ernzerhof, *Phys. Rev. Lett.*, 1997, **78**, 1396–1396; c) J. P. Perdew, S. Kurth, A. Zupan, and P. Blaha, *Phys. Rev. Lett.*, 1999, **82**, 2544–2547; d) Y. Zhang and W. Yang, *Phys. Rev. Lett.*, 1998, **80**, 890–890.
3. a) P. E. Blöchl, *Phys. Rev. B*, 1994, **50**, 17953–17979. ; (b) G. Kresse and D. Joubert, *Phys. Rev. B*, 1999, **59**, 1758–1775.
4. J. Heyd, G. E. Scuseria and M. Ernzerhof, *J. Chem. Phys.*, 2003, **118**, 8207–8215.
5. M.-S. Liao and S. Scheiner, *J. Chem. Phys.*, 2002, **117**, 205–219.
6. a) F. Furche, R. J. Ahlrichs F. Furche and R. Ahlrichs, *J. Chem. Phys.*, 2002, **117**, 7433–7447; b) S. Grimme, *J. Chem. Phys.*, 2006, **124**, 034108.
7. M. J. Frisch, G. W. Trucks, H. B. Schlegel, G. E. Scuseria, M. A. Robb, J. R. Cheeseman, G. Scalmani, V. Barone, G. A. Petersson, H. Nakatsuji, X. Li, M. Caricato, A. Marenich, J. Bloino, B. G. Janesko, R. Gomperts, B. Mennucci, H. P. Hratchian, J. V. Ortiz, A. F. Izmaylov, J. L. Sonnenberg, D. Williams-Young, F. Ding, F. Lipparini, F. Egidi, J. Goings, B. Peng, A. Petrone, T. Henderson, D. Ranasinghe, V. G. Zakrzewski, J. Gao, N. Rega, G. Zheng, W. Liang, M. Hada, M. Ehara, K. Toyota, R. Fukuda, J. Hasegawa, M. Ishida, T. Nakajima, Y. Honda, O. Kitao, H. Nakai, T. Vreven, K. Throssell, J. A. Montgomery, Jr., J. E. Peralta, F. Ogliaro, M. Bearpark, J. J. Heyd, E. Brothers, K. N. Kudin, V. N. Staroverov, T. Keith, R. Kobayashi, J. Normand, K. Raghavachari, A. Rendell, J. C. Burant, S. S. Iyengar, J. Tomasi, M. Cossi, J. M. Millam, M. Klene, C. Adamo, R. Cammi, J. W. Ochterski, R. L. Martin, K. Morokuma, O. Farkas, J. B. Foresman, and D. J. Fox, Gaussian 09, Revision B.01, Wallingford CT (**2009**).

8. H. Arjun, K. Sharath, B. B. P., K. Gagandeep, R. N. Chaki, A. Matthew, S. J. K., B. Subhrashis, V. Kumar, H. Thomas, V. Sandeep and B. Rahul, *Angew. Chem. Int. Ed.*, 2016, **55**, 7806–7810.
9. R. B. Weisenfeld, *Bioorganic Med. Chem.*, 2007, **15**, 6361–6366.
10. M. E. Lalande, V. Ling, R. G. Miller, *Proc Natl Acad Sci U S A.* 1981; **78**, 363–367.